Journal of Materiomics 5 (2019) 404–412

Contents lists available at ScienceDirect

Journal of Materiomics

journal homepage: www.journals.elsevier.com/journal-of-materiomics/

First-principles prediction of magnetically ordered half-metals above room temperature

Muhammad Atif Sattar [a, b], S. Aftab Ahmad [a], Fayyaz Hussain [c], Claudio Cazorla [b, *]

[a] Department of Physics, The Islamia University of Bahawalpur, 63100, Bahawalpur, Pakistan
[b] School of Materials Science and Engineering, UNSW Sydney, NSW, 2052, Australia
[c] Department of Physics, Bahauddin Zakariya University, 60800, Multan, Pakistan

ARTICLE INFO

Article history:
Received 21 February 2019
Received in revised form
29 March 2019
Accepted 7 April 2019
Available online 11 April 2019

ABSTRACT

Half-metallicity (HM) offers great potential for engineering spintronic applications, yet only few magnetic materials present metallicity in just one spin channel. In addition, most HM systems become magnetically disordered at temperatures well below ambient conditions, which further hinders the development of spin-based electronic devices. Here, we use first-principles methods based on density functional theory (DFT) to investigate the electronic, magnetic, structural, mixing, and vibrational properties of 90 *XYZ* half-Heusler (HH) alloys (X = Li, Na, K, Rb, Cs; Y = V, Nb, Ta; Z = Si, Ge, Sn, S, Se, Te). We disclose a total of 28 new HH compounds that are ferromagnetic, vibrationally stable, and HM, with semiconductor band gaps in the range of 1–4 eV and HM band gaps of 0.2–0.8 eV. By performing Monte Carlo simulations of a spin Heisenberg model fitted to DFT energies, we estimate the Curie temperature, T_C, of each HM compound. We find that 17 HH HM remain magnetically ordered at and above room temperature, namely, $300 \leq T_C \leq 450$ K, with total magnetic moments of 2 and 4 μ_B. A further materials sieve based on zero-temperature mixing energies let us to conclude 5 overall promising HH HM that remain magnetically ordered at and above room temperature: NaVSi, RbVTe, CsVS, CsVSe, and RbNbTe. We also predict 2 semiconductor materials that are ferromagnetic at ambient conditions: LiVSi and LiVGe.

1. Introduction

Half-metals (HM) with full spin polarization at the Fermi level are of great potential for spintronic and energy conversion applications [1–3]. In particular, HM are considered to be ideal for injecting spin-polarized currents into semiconductors [4,5] and for manufacturing electrodes to be used in magnetic tunnel junctions and giant magnetoresistance devices [6,7]. Half-Heusler (HH) alloys comprise a relatively large family of multifunctional materials with chemical formula *XYZ* and cubic symmetry (space group $F\bar{4}3m$); the archetypal HH compound NiMnSb was the first half-metal material to be ever reported [8]. The structural compatibility of HH HM with typical cubic semiconductors along with the potentially huge number of current HH HM compounds [9] and the possibility of combining different HH to form HM layered structures [10], open great prospects in the field of spin-based electronics.

In recent years, HH alloys have been studied extensively with computational first-principles methods [11,12]. The structural simplicity, rich variety, and predictable electronic behaviour (e.g., modified Slater-Pauling rule [13]) of HH alloys convert these materials into a perfect target for automated computational searches of HM [14–16]. The energy, electronic, and magnetic properties of HH calculated at zero temperature are the usual materials descriptors employed to guide the theoretical searches of candidate HM. However, analysis of the corresponding magnetic properties at room temperature, which are crucial for the engineering of practical applications [17,18], usually are neglected due to the large computational load associated with first-principles simulation of thermal effects [19]. Furthermore, ferromagnetic (FM) spin ordering is widely assumed in such computational investigations [20,21] regardless of the fact that anti-ferromagnetic (AFM) spin ordering is also possible in half-metals [13,22–24]. In order to provide improved guidance to future experiments, it is convenient then to examine the magnetic properties of HH HM at $T \neq 0$ K conditions, besides their vibrational and mixing stabilities.

* Corresponding author.
E-mail address: c.cazorla@unsw.edu.au (C. Cazorla).
Peer review under responsibility of The Chinese Ceramic Society.

https://doi.org/10.1016/j.jmat.2019.04.003

In this article, we investigate the electronic, magnetic, structural, mixing, and vibrational properties of 90 *XYZ* HH alloys (X = Li, Na, K, Rb, Cs; Y = V, Nb, Ta; Z = Si, Ge, Sn, S, Se, Te) with first-principles methods based on density functional theory (DFT). Our selection of materials has been motivated by recent results reported by other authors for similar compounds [13,25,26]. We introduce a simple HH spin Heisenberg model fitted to FM and AFM DFT energies that permits fast and systematic monitoring of the magnetisation as a function of temperature. We predict that a total of 17 HH HM are vibrationally stable and remain magnetically ordered at and above room temperature, with total magnetic moments of 2 and 4 μ_B and semiconductor (half-metal) band gaps in the range of 1–4 (0.2–0.8) eV. A further materials sieve based on zero-temperature mixing energies leads us to identify the 5 most promising HH HM for spintronic applications. Meanwhile, a total of 21 HH alloys are found to be AFM but all of them turn out to be metallic. We also predict 2 new FM semiconductors with high thermodynamic stability and Curie temperatures. General structural, thermodynamic, and functional trends are identified across the *X*, *Y*, and *Z* series.

2. Methods

In what follows, we explain the technical details of our first-principles calculations. We also describe the simple spin Heisenberg model that we have devised to analyse the magnetic properties of HH alloys at finite temperatures, along with the technical details of the accompanying Monte Carlo simulations.

2.1. First-principles calculations

Density functional theory (DFT) calculations have been performed with the self-consistent full potential linearized augmented plane wave (FP-LAPW) method, as implemented in the WIEN2K code [28]. The generalised gradient approximation to the exchange-correlation energy due to Perdew-Burke-Ernzerhof (PBE) [29] has been employed in this study to estimate energies and determine equilibrium geometries. The value of the $R \times mtK_{max}$ product, where R_{mt} is the value of the muffin-tin sphere radii and K_{max} of the plane wave cut-off energy, was fixed to 9 in order to provide highly converged results. Likewise, a dense **k**-point mesh of $21 \times 21 \times 21$ was used for integrations within the first Brillouin zone (IBZ). The self-consistent threshold values adopted for the calculation of energies and equilibrium geometries were 10^{-5} eV and 10^{-4} eV/Å, respectively. In order to estimate accurate electronic and magnetic properties (e.g., band gaps and magnetic moments) at reasonable computational cost, we employed the Tran-Blaha modified Becke-Johnson (TB-mBJ) *meta*-GGA exchange-correlation functional [30] over the equilibrium structures generated with PBE.

The pseudopotential plane-wave DFT code VASP [31] has been also used for determining the energy difference between FM and AFM spin orderings, and for estimating vibrational lattice phonons. We used the projector-augmented wave method to represent the ionic cores [32], considering the following electrons as valence states: *X s*, *p*, and *d*; *Y s*, *p*, and *d*; and *Z s* and *p*. Wave functions were represented in a plane-wave basis truncated at 650 eV, and for integrations within the IBZ we employed a dense Γ-centered **k**-point mesh of $16 \times 16 \times 16$. The calculation of phonon frequencies was performed with the small displacement method [33] and the PHONOPY code [34]. The following parameters provided sufficiently well converged phonon frequencies: 192–atom supercells (i.e., $4 \times 4 \times 4$ replication of the conventional HH unit cell containing three atoms), Γ-centered **k**-point mesh of $4 \times 4 \times 4$, self-consistent threshold value of 10^{-7} eV, and atomic displacements of 0.02 Å.

2.2. Spin heisenberg model and Monte Carlo simulations

To analyse the effects of temperature on the magnetic properties of HH alloys, we define the following spin Heisenberg Hamiltonian:

$$E_{spin} = E_0 + \frac{1}{2}\sum_{ij} J_{ij} S_i S_j \,, \tag{1}$$

where E_0 is a reference energy, S_i represents the magnetic moment of ion i, and J_{ij} the exchange interactions of the ion i with the rest. In our model, we only consider spin couplings between nearest magnetic ions (which add up to 12, given that the symmetry of the magnetic sublattice is face centered cubic) and assume that all exchange interactions are equal. Based on such simplifications, the value of the model parameters can be calculated straightforwardly with DFT methods as:

$$\begin{aligned} E_0 &= \frac{1}{4}(E_{FM} + 3E_{AFM}) \\ J_{ij} &= \frac{1}{8|S|^2}(E_{FM} - E_{AFM}) \,, \end{aligned} \tag{2}$$

where E_{FM} and E_{AFM} are the energy of the crystal considering perfect ferromagnetic and anti-ferromagnetic spin arrangements, respectively. (We recall that in the AFM spin configuration each magnetic ion sees 8 out of its 12 nearest neighbors with opposite spin orientation [35].)

Classical Monte Carlo (MC) simulations of the spin Heisenberg Hamiltonian just explained were performed to estimate the magnetisation of HH alloys (that is, equal to the sum of all individual spins) as a function of temperature. We used a periodically-repeated simulation box containing $20 \times 20 \times 20$ spins. Thermal averages were computed from runs of 50,000 MC sweeps performed after equilibration (which consisted of the same number of MC steps). A small symmetry-breaking magnetic anisotropy was introduced in the MC simulations to facilitate the accompanying numerical analysis [36]. By using this setup and monitoring the evolution of the magnetisation as a function of T, we were able to estimate magnetic transition temperatures, T_C, with a numerical accuracy of 25 K.

It is worth noting that in spite of the simplicity of the spin Heisenberg Hamiltonian adopted here, similar models have been able to provide accurate results for the T-induced variation of the magnetisation in complex magnetic materials (e.g., multiferroic oxide perovskites [37–39]). To check the reliability of the simple spin-interaction model introduced in this work, we performed a numerical test for the half-metallic and ferromagnetic HH alloy NiMnSb, which displays an experimental Curie temperature of 730 K [40]. Our MC simulations provide $T_C = 615 \pm 25$ K for this material, which indicates that our simple spin Heisenberg Hamiltonian tends to underestimate moderately the Curie temperatures of HH alloys. We should note that this is not a negative outcome in itself since it ensures that the compounds identified as magnetically ordered near room temperature in this work are very likely to continue being so at higher temperatures.

3. Results and discussion

We start this section by providing an overview of the computational strategy that we have followed to determine the ground-state configurations of HH alloys, and the general classification that results from our calculations based on their structural,

electronic, and magnetic properties. Then, we explain in detail the electronic and vibrational properties of the disclosed HH HM, followed by a discussion on their magnetic phase transition temperatures and zero-temperature mixing energies. Finally, we highlight the *XYZ* HH (X = Li, Na, K, Rb, Cs; Y = V, Nb, Ta; Z = Si, Ge, Sn, S, Se, Te) alloys that according to our calculations are most promising for spintronic applications.

3.1. Overview of the 90XYZ HH alloys

The *XYZ* HH alloys considered in this study feature an alkali metal in the *X* position (Li, Na, K, Rb, and Cs), a transition metal in the *Y* position (V, Nb, and Ta), and a non-metal *sp*-element in the *Z* position (Si, Ge, Sn, S, Se, and Te). The cubic HH unit cell consists of three interpenetrating face centered cubic (fcc) sublattices that together render a crystal structure with $F\bar{4}3m$ symmetry. There exist three possible inequivalent atomic structures compatible with this geometry, namely, T1, T2, and T3, which are generated by permuting the *X*, *Y*, and *Z* ions over the Wyckoff positions $4a\ (0,0,0)$, $4b\ \left(\frac{1}{2},\frac{1}{2},\frac{1}{2}\right)$, and $4c\ \left(\frac{1}{4},\frac{1}{4},\frac{1}{4}\right)$ (see Fig. 1 and caption therein) [27]. The physical properties of HH alloys may be greatly influenced by their specific atomic arrangement [16,27]; for instance, we have found here that some electronic features of interest may change noticeably depending on the selected geometry (as it will be shown later). Consequently, configurations T1, T2, and T3 need to be all considered when performing systematic computational searches in *XYZ* HH alloys.

Systematic fixed-volume geometry optimizations have been carried out for each HH compound to determine the energetically most favorable atomic arrangement, equilibrium volume, and magnetic ordering. First, the equilibrium volume of each possible structure considering FM spin ordering is obtained by fitting the series of calculated energy points to a Birch-Murnaghan equation of state [41]; subsequently, the energy associated with AFM spin ordering is analysed for the lowest-energy atomic arrangement obtained in the FM case. Fig. 2a–b illustrate such a computational procedure for the particular case of NaVTe, which turns out to exhibit a T1–FM ground state and an equilibrium volume of 320 Å^3. Once the optimal atomic arrangement, equilibrium volume, and magnetic ordering have been determined at the PBE level, we accurately calculate the corresponding electronic properties (e.g., energy band gaps and magnetic moments) with the TB-mBJ functional [30].

Fig. 3 shows a general classification of the 90 HH compounds analysed in this study made on basis to their structural, magnetic, and electronic properties. A total of 56 materials present lowest energy on the T1 arrangement, 32 on the T3, and only 2 on the T2. Compounds with a light-weight and small-radius alkali metal in the *X* position (e.g., Li, Na, and K) tend to be more stable in the T1 arrangement, whereas those with heavy-weight and large-radius alkali metals (e.g., Rb and Cs) in the T3. On the other hand, compounds with a heavy-weight and large-radius transition metal in the *Y* position (e.g., Nb and Ta) mostly are stabilized in the T1 configuration, made the exception of the HH alloys containing Cs

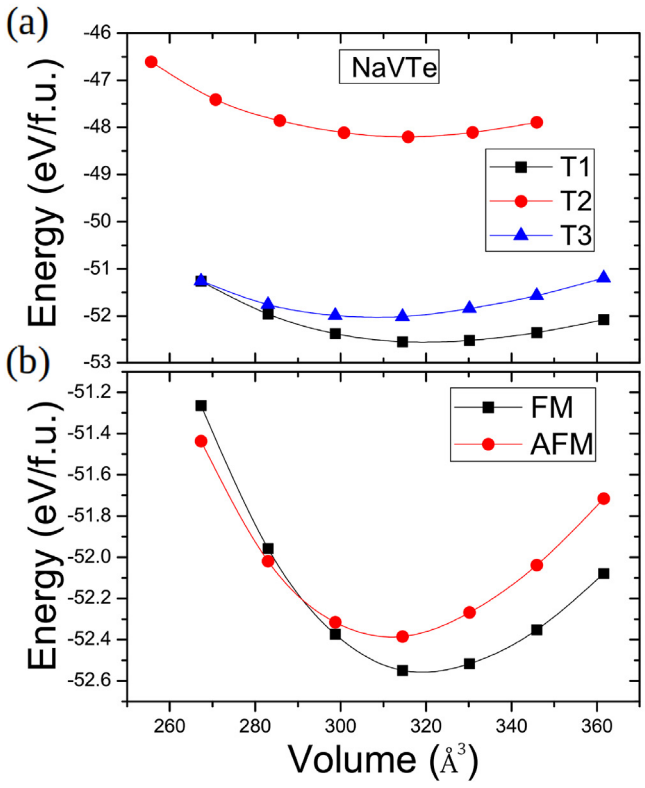

Fig. 2. Volume optimization of the HH alloy NaVTe. (a) Three different atomic structures are considered with fixed ferromagnetic (FM) spin ordering. (b) Ferromagnetic and anti-ferromagnetic (AFM) spin orderings are considered in the lowest-energy T1 structure.

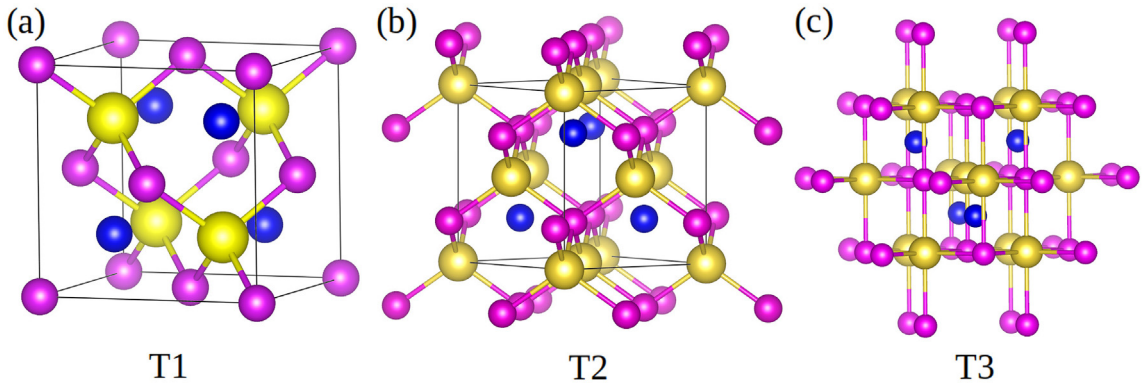

Fig. 1. Conventional unit cell of *XYZ* HH alloys (cubic symmetry, space group $F\bar{4}3m$) considering the three possible inequivalent atomic arrangements [27]. (a) T1 with *X*'s Wyckoff positions $4a\ (0,0,0)$, *Y*'s $4b\ \left(\frac{1}{2},\frac{1}{2},\frac{1}{2}\right)$, and *Z*'s $4c\ \left(\frac{1}{4},\frac{1}{4},\frac{1}{4}\right)$. (b) T2 with *X*'s Wyckoff positions $4b\ \left(\frac{1}{2},\frac{1}{2},\frac{1}{2}\right)$, *Y*'s $4c\ \left(\frac{1}{4},\frac{1}{4},\frac{1}{4}\right)$, and *Z*'s $4a\ (0,0,0)$. (c) T3 with *X*'s Wyckoff positions $4c\ \left(\frac{1}{4},\frac{1}{4},\frac{1}{4}\right)$, *Y*'s $4a\ (0,0,0)$, and *Z*'s $4b\ \left(\frac{1}{2},\frac{1}{2},\frac{1}{2}\right)$. Yellow, blue, and pink spheres represent *X*, *Y*, and *Z* ions, respectively. Neighbouring *X* and *Z* ions are joint by *rods* in order to facilitate the visualisation of the three-dimensional structures (that is, they do not represent real bonds).

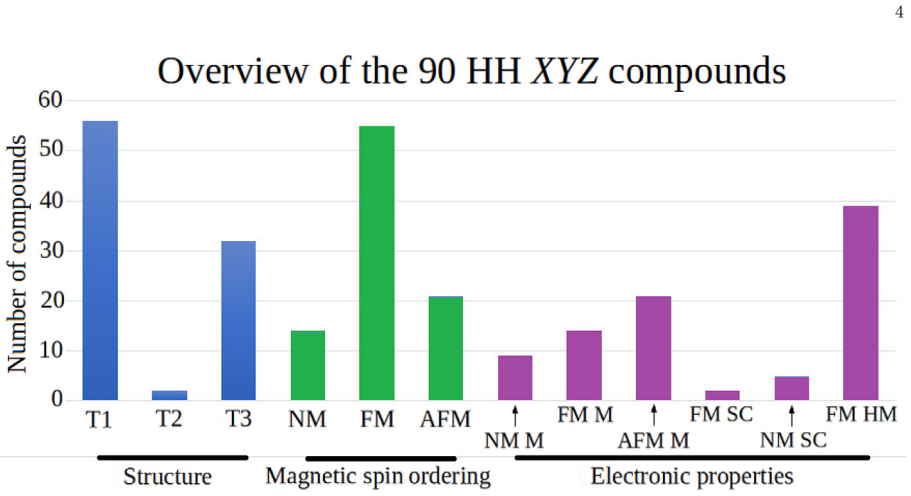

Fig. 3. Properties summary of the 90 HH *XYZ* alloys analysed in this study for their lowest-energy configuration. Magnetic spin ordering is classified into non-magnetic (NM), ferromagnetic (FM), and anti-ferromagnetic (AFM). Electronic properties are described as metallic (M), semiconductor (SC), and half-metallic (HM).

which always adopt the T3 arrangement. Meanwhile, the role of the non-metal element occupying the *Z* position on determining the most favorable structure appears to be negligible. We note that the two compounds that adopt the T2 configuration turn out to be metallic (i.e., LiTaSn and LiNbSn); thereby, the T2 arrangement will be ignored for the remainder of this article. Overall, these results indicate that the main reason for the HH alloys analysed in this study to choose either the T1 or T3 structure is the relative weight/size difference between the *X* and *Y* cations (i.e., T1 for small mass and size *X* and *Y* ratios whereas T3 for large) [27].

At zero-temperature conditions, we find that 55 HH alloys are FM, 21 AFM, and 14 non-magnetic (see Fig. 3). A total of 39 FM compounds are found to be half-metallic, 2 FM semiconductor (SC), and the rest metallic. In what follows, we describe with detail the electronic, vibrational, magnetic, and mixing properties of the 41 new HM and SC compounds that have been determined in our investigation, all of which present FM spin ordering.

3.2. Electronic and vibrational properties

Fig. 4 shows the energy and half-metallic band gaps, E_{BG} and E_{HM}, estimated for the 90 *XYZ* HH alloys considered in this study. E_{BG} is the energy difference between the top of the valence band and bottom of the conduction band in the semiconductor spin channel, and E_{HM} the minimum energy that an electron requires to surpass the spin gap (see Fig. 5, where we represent those quantities for CsVSe). One can observe a certain correlation between these two quantities, namely, large E_{BG}'s are accompanied by large E_{HM}'s. For instance, RbNbS (T1 arrangement) has an energy band gap of 5.08 eV and HM band gap of 1.46 eV, while CsVSn (T3 arrangement) has 1.30 eV and 0.18 eV, respectively. Nevertheless, there are few compounds that in spite of having a relatively small energy band gap exhibit a relatively large HM band gap (e.g., RbNbSi in the T3 configuration for which we estimate $E_{BG} = 1.24$ eV and $E_{HM} = 0.57$ eV).

The color code employed in Fig. 4 shows that the HH alloys consisting of heavy-weight *X*-ions (K, Rb, and Cs), light-weight *Y*-ions (V and Nb), and chalcogen elements (S, Se, and Te) in the *Z* position, generally possess the largest E_{BG} and E_{HM}. By contrast, HH compounds with a light-weight (heavy-weight) alkali (transition) metal element like Li (Ta) in the *X* (*Y*) position mostly are metallic or present medium band gaps.

Fig. 6 shows the spin-projected density of electronic states calculated for the ground state of RbVTe (T3 configuration). This

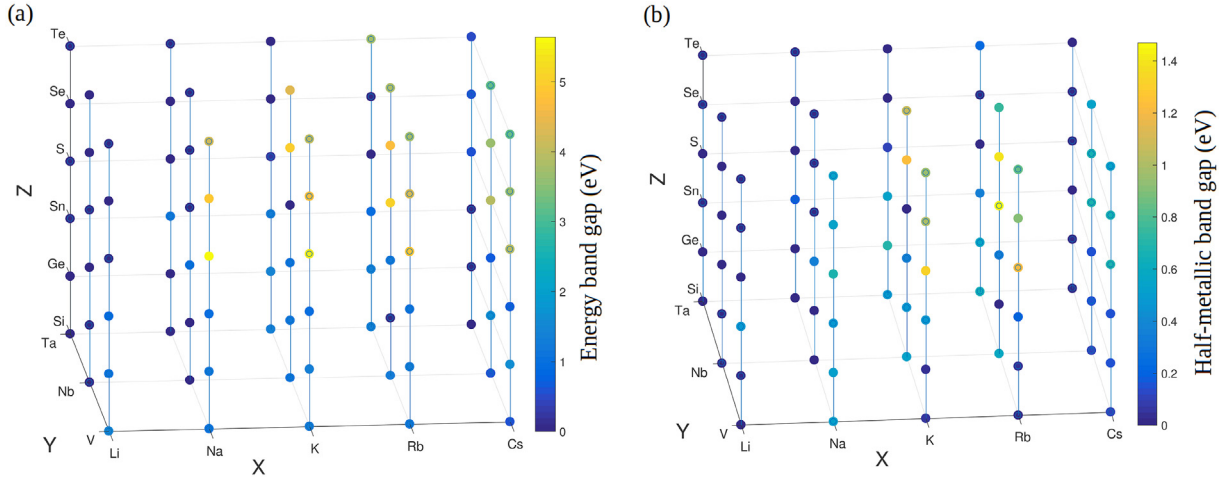

Fig. 4. Electronic properties of the 90 HH *XYZ* alloys analysed in this study for their lowest-energy configuration. (a) Energy band gap, E_{BG}, and (b) half-metallic band gap, E_{HM}. Blue and yellow colors denote smaller and larger band gap values, respectively, and the integrating *X*, *Y*, and *Z* species are indicated in the three orthogonal axis.

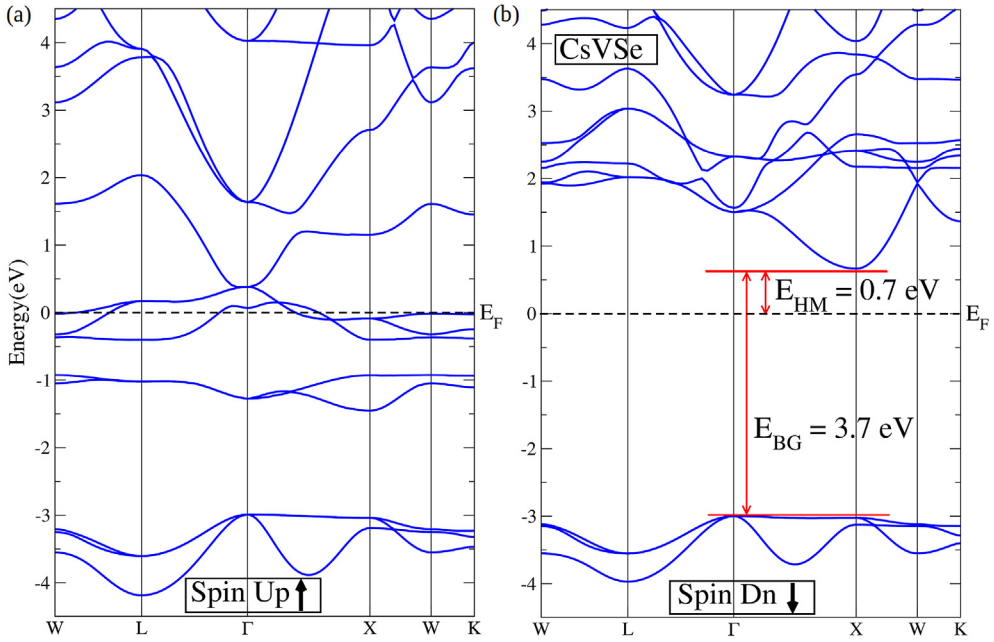

Fig. 5. Band structure of the half-metallic HH alloy CsVSe (T3 arrangement) predicted in this study; the horizontal dashed line represents the Fermi level, E_F, which has been shifted to zero. CsVSe is vibrationally stable at Γ, displays FM spin ordering with a Curie temperature of $T_C = 375\pm25$ K, possesses a relatively small zero-temperature mixing energy of 0.11 eV/atom, and has a total magnetic moment of 4 μ_B. The energy band gap of CsVSe is 3.66 eV and the accompanying half-metallic band gap is 0.66 eV. The electronic properties are calculated with the Tran-Blaha modified Becke-Johnson (TB-mBJ) *meta*-GGA exchange-correlation functional [30].

compound is half-metallic with a large E_{HM} of 0.83 eV and large energy band gap of 3.73 eV, hence is an interesting case for which to analyse the electronic features. In the majority band (spin up), is appreciated that the V d–t_{2g} and Rb d orbitals are highly hybridised in the region surrounding the Fermi level, which leads to the appearance of metallicity in that channel. In the minority band (spin down), however, the V and Rb d orbitals are shifted to higher energies and remain unoccupied; consequently, a HM band gap appears in that channel between the occupied d bonding and unoccupied d antibonding states. Meanwhile, the majority of states forming the top of the valence band in the minority band (spin down) correspond to Te p orbitals, which are shifted to energies well below those of the V and Rb d orbitals.

It is worth noting that if the higher-energy configuration T1 is considered instead of the lowest-energy configuration T3, the hybridisation between electronic orbitals in RbVTe does not change appreciably; however, the resulting energy band gaps E_{BG} and E_{HM} increase by 7 and 20%, respectively, as compared to the T3 case. These results illustrate very well the need to consider all possible inequivalent atomic arrangements when performing systematic analysis in *XYZ* HH alloys, in order to determine the correct ground-state properties.

We note that when the chalcogen element (S, Se, and Te) in the Z position is substituted by a group–XIV element (Si, Ge, Sn), E_{BG} and E_{HM} generally undergo a significant reduction (see Fig. 4). For instance, RbVSn has an energy band gap of 1.13 eV and a HM band gap of 0.20 eV. Such a band gap closure is consequence of a decrease in the energy separation between the Z p orbitals and X–Y d bonding and antibonding states (not shown here), and it occurs when the number of valence electrons in the system changes from 12 (S, Se, Te) to 10 (Si, Ge, Sn). Interestingly, the energy band gap changes as induced by Z–element substitutions correlate directly with changes in the magnetic moment of the ions; we will discuss in detail this and other magnetic effects in the next subsection.

Out of the 90 HH alloys investigated in this study, we have found that 39 (2) are ferromagnetic and half-metallic (magnetic semiconductor) at zero-temperature conditions. In order to provide useful guidance for the experiments, it is necessary also to assess the vibrational stability of the candidate materials proposed by theory. Here, we have calculated the lattice phonons for each HH alloy at the high-symmetry reciprocal point Γ, and concluded that 28 FM HM along with the 2 FM SC are vibrationally well behaved (that is, do not present imaginary phonon frequencies at the IBZ centre). For some selected cases (namely, the overall most promising materials that will be discussed in Sec. III D), we have calculated also the full phonon spectrum over the entire IBZ and found that most of them are vibrationally stable (see Fig. 7, where we enclose a couple of relevant cases). We have not been able to draw any robust correlation between vibrational instability and chemical structure for the HH alloys analysed in this study. For the remainder of the article, we will focus on describing the magnetic and mixing properties of the 28 (2) FM, HM (SC), and vibrationally stable (at Γ, at least) compounds that we have predicted.

3.3. Magnetism and mixing stability

Recently, Damewood et al. [13] have proposed a modified Slater-Pauling (mSP) rule for describing the magnetic moment of the half-Heusler alloys LiMnZ (Z = N, P, Si). Specifically, the total magnetic moment per formula unit (expressed in units of μ_B), M, has been parametrised as:

$$M = N_t - 8\,, \tag{3}$$

where N_t is the total number of valence electrons in the unit cell. In the present case, N_t is equal to 12 for alloys displaying S, Se, or Te in the Z position, and to 10 for Si, Ge, and Sn (we recall that $N_t = 1$ for the X elements considered in this study, $N_t = 5$ for the Y's, and $N_t = 4$ or 6 for the Z's). We have found that all non-metallic and magnetic *XYZ* alloys disclosed in this study (i.e., either HM or SC) in fact follow the mSP rule proposed by Damewood et al. [13] (some examples are provided in Table 1). Interestingly, in those cases we also

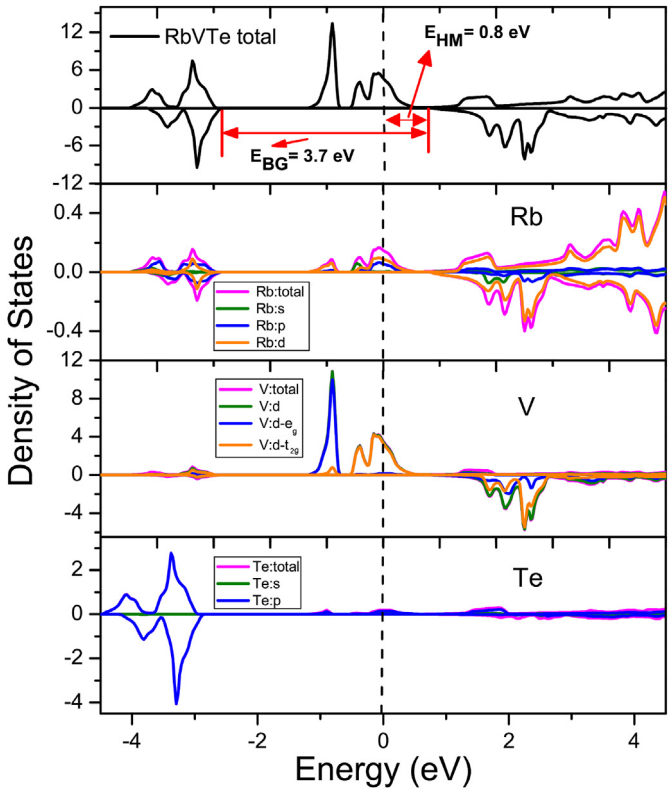

Fig. 6. Spin-projected total and partial density of states of the half-metallic HH alloy RbVTe (T3 arrangement) predicted in this study; spin up (down) density components are represented in the positive (negative) panels. The horizontal dashed line represents the Fermi level, which has been shifted to zero. RbVTe is vibrationally stable at Γ, displays FM spin ordering with a Curie temperature of $T_C = 375\pm25$ K, possesses a relatively small zero-temperature mixing energy of 0.14 eV/atom, and has a total magnetic moment of 4 μ_B. The energy band gap of RbVTe is 3.73 eV and the accompanying half-metallic band gap is 0.83 eV. The electronic properties are calculated with the Tran-Blaha modified Becke-Johnson (TB-mBJ) *meta*-GGA exchange-correlation functional [30].

observe a clear correlation between the total magnetisation and size of the energy band gap: large M's and large E_{BG}'s occur simultaneously in the same compounds. From an applied point of view, this seems to be a positive finding since wide band gap HM alloys are likely to be also magnetically robust. Nevertheless, the size of the magnetic moments does not provide any information on the variation of the magnetisation as a function of temperature, which is mostly related to the exchange interactions between magnetic moments.

We have estimated the magnetic transition temperature, T_C, for the 28 (2) FM, HM (SC), and Γ vibrationally stable compounds determined in this study, by using the computational methods explained in Sec. II B. Our T_C results are shown in Fig. 8. It is appreciated that compounds with a heavy-weight alkali metal in the X position (Rb and Cs) concentrate the highest magnetic transition temperatures (see also Table 1). For instance, RbNbTe displays a Curie temperature of 450±25 K and CsVSe of 375±25 K, while NaVTe becomes paramagnetic at 150±25 K and KTaGe at 225±25 K. We ascertain the lack of any correlation between the size of the ionic magnetic moments, M, and the Curie temperature of the system; for example, RbNbSn displays $M = 2\ \mu_B$ and $T_C = 450\pm25$ K while for RbNbTe we estimate $M = 4\ \mu_B$ and the same magnetic transition temperature. Interestingly, we find that a total of 17 (2) FM and HM (SC) compounds, which as we have checked are vibrationally stable over the whole IBZ, remain magnetically ordered at or above room temperature. All of them are listed in Table 1 and will be discussed in the next subsection.

Finally, we calculated the zero-temperature mixing energy, E_{mix}, of the 28 (2) FM, HM (SC), and vibrational stable compounds disclosed in this work, by using the formula:

$$E_{mix} = E^{HH}_{XYZ} - \left(E^{fcc}_X + E^{fcc}_Y + E^{fcc}_Z\right), \quad (4)$$

where E^{HH}_{XYZ} represents the ground-state energy of the HH alloy, and E^{fcc}_A the energy of the bulk A crystal considering an equilibrium fcc structure (due to computational load constraints, we have systematically neglected the existence of other possible competing phases in our mixing stability analysis). E_{mix} provides a quantitative estimation of how stable the XYZ system is against decomposition into X-, Y–, and Z-rich regions. In particular, negative (positive) values of the mixing energy indicate high (low) stability of the compound against phase decomposition.

Here, we (somewhat arbitrarily) consider that a E_{mix} threshold value of 200 meV per formula unit (or, equivalently, 67 meV per atom) can be used to sieve materials with reasonably good mixing stability from those with tendency for phase separation. This numerical choice is based on the fact that in our DFT calculations we are neglecting few possible temperature effects that may have a stabilising impact on the analysed HH alloys when considering

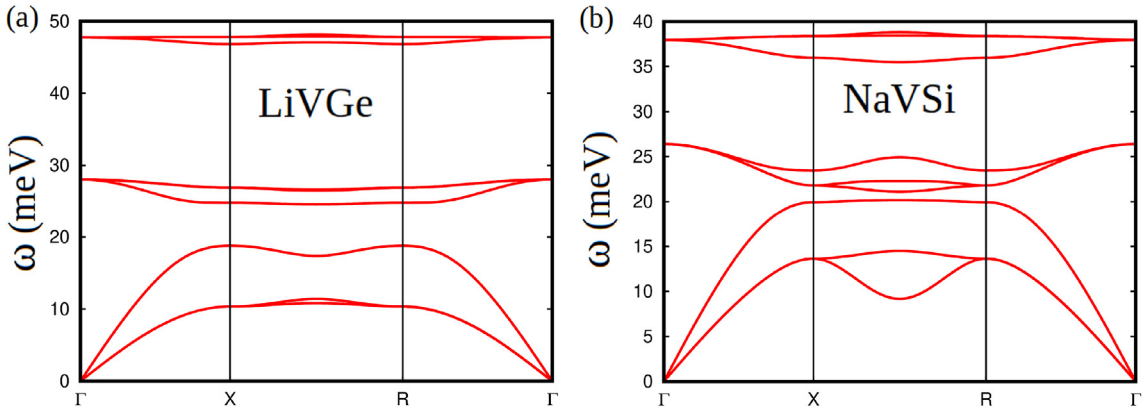

Fig. 7. Phonon spectrum of the semiconductor and half-metallic HH alloys LiVGe and NaVSi (both in the T1 arrangement) predicted in this study. (a) LiVGe is vibrationally stable, displays FM spin ordering with a Curie temperature of $T_C = 375\pm25$ K, possesses a zero-temperature mixing energy of −0.11 eV/atom, a total magnetic moment of 2 μ_B, and an energy band gap of 1.06 eV. (b) NaVSi is vibrationally stable, displays FM spin ordering with a Curie temperature of $T_C = 300\pm25$ K, possesses a relatively small zero-temperature mixing energy of 0.21 eV/atom, a total magnetic moment of 2 μ_B, an energy band gap of 1.11 eV, and an accompanying half-metallic band gap of 0.52 eV.

Table 1
Properties summary of the most relevant HH alloys predicted in this study considering their lowest-energy configuration. The 7 overall most promising HH compounds are highlighted in bold. All systems are vibrationally stable and display FM spin ordering. The electronic properties are calculated with the Tran-Blaha modified Becke-Johnson (TB-mBJ) *meta*-GGA exchange-correlation functional [30]. The numerical uncertainty in our T_C results is ±25 K.

Compound	Structure	a_0 (Å)	Electronic behavior	M (μ_B)	E_{BG} (eV)	E_{HM} (eV)	T_C (K)	E_{mix} (eV/f.u.)
LiVSi	T1	5.85	**SC**	**2.0**	**1.43**	–	**300**	− 0.11
LiVGe	T1	5.93	**SC**	**2.0**	**1.06**	–	**375**	− 0.11
NaVSi	T1	6.25	**HM**	**2.0**	**1.11**	**0.52**	**300**	+ 0.21
NaVTe	T1	6.84	HM	4.0	4.18	0.54	150	− 0.12
KVSi	T3	6.55	HM	2.0	1.49	0.21	375	+ 0.56
RbVTe	T3	7.27	**HM**	**4.0**	**3.73**	**0.83**	**375**	+ 0.14
CsVS	T3	6.93	**HM**	**4.0**	**3.92**	**0.68**	**300**	+ 0.01
CsVSe	T3	7.13	**HM**	**4.0**	**3.66**	**0.66**	**375**	+ 0.11
RbNbSi	T3	6.77	HM	2.0	1.24	0.57	450	+ 0.83
RbNbSn	T3	7.19	HM	2.0	1.19	0.33	450	+ 0.83
RbNbTe	T3	7.41	**HM**	2.0	**3.82**	**0.75**	**450**	+ 0.40
CsNbSi	T3	6.87	HM	2.0	0.47	0.11	375	+ 0.91
CsNbGe	T3	6.96	HM	2.0	0.62	0.14	375	+ 0.91
CsNbSn	T3	7.28	HM	2.0	0.69	0.16	375	+ 0.94
CsNbTe	T3	7.55	HM	4.0	3.23	0.39	450	+ 0.49
KTaSn	T1	7.17	HM	2.0	1.31	0.54	300	+ 0.88
RbTaSi	T1	6.89	HM	2.0	1.36	0.66	300	+ 0.92
RbTaGe	T1	6.99	HM	2.0	1.39	0.55	300	+ 0.97
RbTaSn	T3	7.16	HM	2.0	1.05	0.35	375	+ 1.03
RbTaTe	T3	7.37	HM	4.0	3.70	0.24	375	+ 0.75

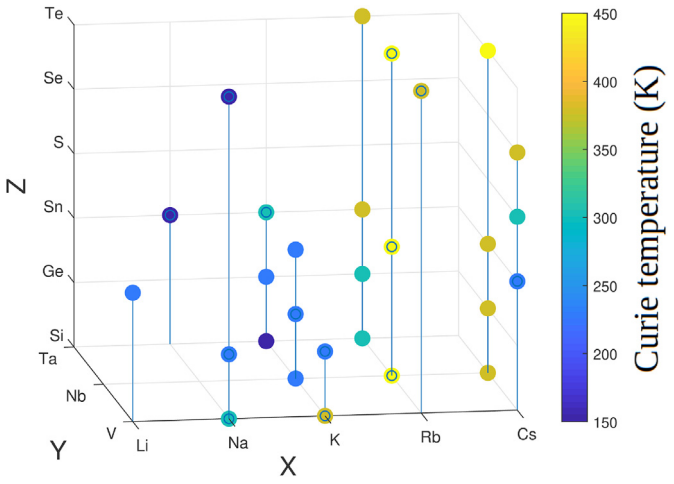

Fig. 8. Curie temperature, T_C, of the 28 half-metallic HH alloys found in this study to be vibrationally stable at Γ and which display FM spin ordering. Yellowish color indicates magnetic transition points above room temperature; the numerical uncertainty in our T_C results is ±25 K.

realistic thermodynamic conditions. For instance, HH alloys typically are synthesised by high-T techniques like arc-melting that naturally lead to some intrinsic atomic disorder [27]; such intrinsic atomic disorder will normally be accompanied by some configurational entropy that will tend to further stabilise the alloy [42,43]. Vibrational contributions to the mixing free energy, which have been totally neglected in the present study, may also have an stabilising effect in the alloys; the magnitude of those free energy contributions may easily amount to ∼ 10 meV/atom [44,45]. Last but not least, it has been shown that the zero-kelvin energies computed with DFT methods sometimes may be not sufficient to correctly describe the most stable phases of Half-Heusler alloys at standard conditions: the discrepancies with respect to experiments may reach up to 300 meV/atom [46].

Fig. 9 shows our E_{mix} results; only 7 compounds out of 30 (i.e., 28 HM and 2 SC) display zero-temperature mixing energies below 0.2 eV per formula unit. We note that all those low mixing energy compounds contain V in the Y position, namely, LiVSi (SC), LiVGe (SC), NaVTe (HM), NaVSi (HM), RbVTe (HM), CsVS (HM), and CsVSe (HM) (see Table 1). Specifically, only the first three alloys listed above present negative E_{mix} values, while for CsVS we obtain a practically null mixing energy. On the other hand, KVSi (HM), RbNbTe (HM), and CsNbTe (HM) exhibit mixing energies close to 0.50 eV/f. u., and for the rest of compounds we estimate E_{mix}'s that are close to 1.00 eV per formula unit. These results indicate that most of the HH HM reported in this work, in spite of possessing relatively high Curie temperatures, are likely to present phase separation issues, which is not desirable for practical applications.

Meanwhile, we observe that when the element occupying the Z position in the HH alloy is a chalcogen (S, Se, and Te) the resulting mixing energy is noticeably smaller than when the element belongs to group−XIV of the periodic table (Si, Ge, Sn). For instance, we find that E_{mix} amounts to −0.12 eV/f.u. For NaVTe and to 0.21 eV/f. u. For NaVSi (see Table 1). The same behaviour is observed also in other compounds presenting either Nb or Ta in the Y position (e.g., for

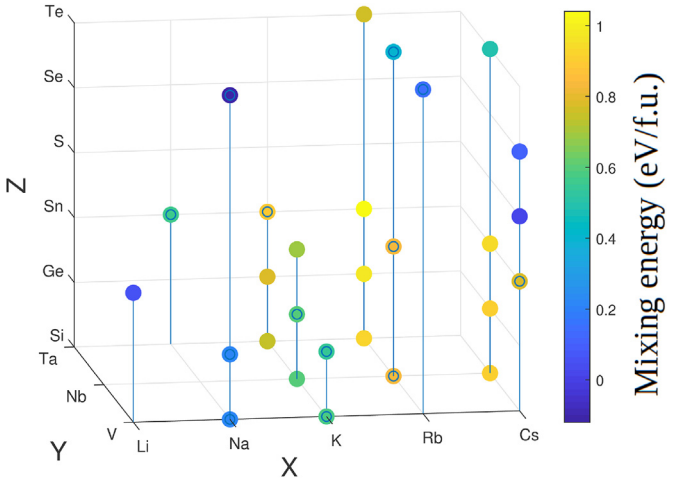

Fig. 9. Zero-temperature mixing energy, E_{mix}, of the 28 half-metallic HH alloys found in this study to be vibrationally stable at Γ and which display FM spin ordering. Bluish color indicates mixing energy values below 0.2 eV per formula unit.

RbTaSn we estimate 1.03 eV/f. u. And for RbTaTe 0.75 eV/f. u.). Therefore, a possible strategy for improving the mixing stability of some of the new HH HM compounds reported in this study (e.g., KVSi with $E_{mix} = 0.56$ eV/f.u. And RbNbSi with $E_{mix} = 0.83$ eV/f.u.) may consist in doping with light-weight alkali metals (Li and Na) in the *X* position (although this may also lead to some unwanted decrease in the energy band gap and Curie temperature of the alloy, see present and previous sections) and/or with chalcogen species in the *Z* position; besides, the configurational entropy resulting from substitutional disorder will tend to further enhance the mixing stability of the formed complex compounds [44]. We note that HM HH doping strategies have been already proposed in the literature and appear to be feasible in practice [47,48].

3.4. Most promising magnetic HH alloys

Table 1 shows the 19 vibrationally stable and ferromagnetic compounds predicted in this study that possess a Curie temperature equal or higher than room temperature. Two out of those 19 alloys are semiconductor while the rest are half-metallic. We have also included NaVTe in the table, in spite of presenting a relatively low Curie temperature of 150 K, owing to its good mixing stability properties ($E_{mix} = -0.12$ eV/f.u.). From an applied perspective, an overall promising HM (or magnetic semiconductor) material should fulfil the following requirements: (1) vibrationally and chemically stable, (2) high Curie temperature, (3) large energy band gaps, (4) large magnetic moment, and (5) structural compatibility with other semiconductor materials typically employed in electronic devices (e.g., silicon and GaAs with respective lattice parameters of 5.4 and 5.6 Å).

Except NaVTe and CsNb*Z* with *Z* = Si, Ge, and Sn, all the compounds reported in Table 1 fulfil conditions (2), (3), and (4) above. Compounds LiVSi (SC), LiVGe (SC), and NaVSi (HM) in addition fulfill (1) and (5), which suggests great potential for spintronic applications [17,18]. Meanwhile, RbVTe (HM), CsVS (HM), and CsVSe (HM) fulfil (1)–(4) and only partially (5); however, the energy band gaps estimated for these compounds are so large that they deserve being highlighted. Finally, we mention RbNbTe as the most encouraging case of HH HM not containing vanadium in the *Y* position; this alloy fulfills conditions (2)–(4), as many others, but the corresponding E_{BG}, E_{HM}, and T_C are exceedingly large.

Overall, the most promising HH alloys for use in spintronic applications predicted by our computational research are LiVSi (SC), LiVGe (SC), NaVSi (HM), RbVTe (HM), CsVS (HM), CsVSe (HM) and RbNbTe (HM), all of which possess magnetic transition temperatures at or above room temperature. The only apparent disadvantage of some of these compounds (i.e., NaVSi and RbNbTe) are their positive mixing energies (see Table 1), which suggests the likely existence of phase separation issues in practice. Nevertheless, as we have mentioned earlier, a likely strategy for solving this particular problem may consist in doping with light-weight alkali metals (Li and Na) in the *X* position, which in turn would improve their structural compatibility with typical semiconductor materials, and/or with chalcogen atoms in the *Z* position [47,48].

4. Conclusions

We have performed a comprehensive first-principles study of the structural, electronic, structural, vibrational, and mixing properties of 90 *XYZ* half-Heusler alloys (*X* = Li, Na, K, Rb, Cs; *Y* = V, Nb, Ta; *Z* = Si, Ge, Sn, S, Se, Te). In contrast to previous computational studies dealing with a large number of candidate materials, we have analysed the magnetic features of most HH alloys at finite temperatures as this piece of information results crucial for reliably guiding the experimental searches of technologically relevant materials. A total of 17 alloys are predicted to be vibrationally stable, half-metallic, and magnetically ordered at room temperature, with total magnetic moments of 2 and 4 μ_B and semiconductor band gaps in the range of 1–4 eV. On the other hand, all the HH alloys that have been identified as anti-ferromagnetic, 21 in total, turn out to be metallic. We have also found 2 new magnetic semiconductors that exhibit high thermodynamic stability and Curie temperatures. Upon analysis of the mixing stability of the vibrationally well-behaved systems, we have identified the following compounds as overall most promising for spintronic applications: LiVSi (SC), LiVGe (SC), NaVSi (HM), RbVTe (HM), CsVS (HM), CsVSe (HM) and RbNbTe (HM). Moreover, we have argued that simple doping strategies may be used to improve the mixing stability of some discarded HH HM presenting convenient electronic and magnetic features. Hence, we hope that our computational study will stimulate new experimental efforts leading to progress in the field of spin-based electronics.

Acknowledgments

This research was supported under the Australian Research Council's Future Fellowship funding scheme (No. FT140100135). M. A. S. acknowledges financial support from the Higher Education Commission (HEC) of Pakistan under the IRSIP scholarship (PIN:IRSIP 35 PSc 11). Computational resources and technical assistance were provided by the Australian Government and the Government of Western Australia through the National Computational Infrastructure (NCI) and Magnus under the National Computational Merit Allocation Scheme and The Pawsey Supercomputing Centre.

References

[1] Felser C, Fecher GH, Balke B. Spintronics: a challenge for materials science and solid-state chemistry. Angew Chem Int Ed 2007;46:668.
[2] Zutic I, Fabian J, Sarma SD. Spintronics: fundamentals and applications. Rev Mod Phys 2003;76:323.
[3] Zhu H, et al. Discovery of TaFeSb-based half-heuslers with high thermoelectric performance. Nat Commun 2019;10:270.
[4] Bhat SG, Anil Kumar PS. Demonstration of efficient spin injection and detection in various systems using Fe_3O_4 based spin injectors. AIP Adv 2016;6:056308.
[5] Dash SP, Sharma S, Patel RS, de Jong MP, Jansen R. Electrical creation of spin polarization in silicon at room temperature. Nature 2009;462:491.
[6] Tanaka CT, Nowak J, Moodera JS. Spin-polarized tunneling in a half-metallic ferromagnet. J Appl Phys 1999;86:6239.
[7] Hordequin C, Nozieres J, Pierre J. Half metallic NiMnSb-based spin-valve structures. J Magn Magn Mater 1998;183:225.
[8] de Groot RA, Mueller FM, van Engen PG, Buschow KHJ. New class of materials: half-metallic ferromagnets. Phys Rev Lett 1983;50:2024.
[9] Casper F, Graf T, Chadov S, Balke B, Felser C. Half-heusler compounds: novel materials for energy and spintronic applications. Semicond Sci Technol 2012;27:063001.
[10] Azadani JG, Munira K, Romero J, Ma J, Sivakumar C, Ghosh AW, et al. Anisotropy in layered half-metallic heusler alloy superlattices. J Appl Phys 2016;119:043904.
[11] Martin R. Electronic structure: basic theory and practical methods. Cambridge University Press; 2012. ISBN:9780511805769.
[12] Cazorla C, Boronat J. Simulation and understanding of atomic and molecular quantum crystals. Rev Mod Phys 2017;89:035003.
[13] Damewood L, Busemeyer B, Shaughnessy M, Fong CY, Yang LH, Felser C. Stabilizing and increasing the magnetic moment of half-metals: the role of Li in half-heusler LiMnZ (Z = N,P,Si). Phys Rev B 2015;91:064409.
[14] Ma J, Hegde VI, Munira K, Xie Y, Keshavarz S, Mildebrath DT, et al. Computational investigation of half-heusler compounds for spintronics applications. Phys Rev B 2017;95:024411.
[15] Legrain F, Carrete J, van Roekeghem A, Madsen GKH, Mingo N. Materials screening for the discovery of new half-heuslers: machine learning versus ab initio methods. J Phys Chem B 2018;122:625.
[16] Sattar MA, Rashid M, Hussain F, Imran M, Hashmi MR, Laref A, et al. Physical properties of half-heusler YMnZ (Z=Si,Ge,Sn) compounds via ab-initio study. Solid State Commun 2018;278:10.
[17] Tu NT, Hai PN, Anh LD, Tanaka M. High-temperature ferromagnetism in heavily Fe-doped ferromagnetic semiconductor (Ga,Fe)Sb. Appl Phys Lett 2016;108:192401.

[18] Cao Q, Fu M, Zhu D, Yao M, Hu S, Chen Y, et al. Growth-controlled engineering of magnetic exchange interactions in single crystalline $GaCoZnO_{1-v}$ epitaxial films with high Co concentration. Chem Mater 2017;29:2717.
[19] Curtarolo S, Hart GLW, Nardelli MB, Mingo N, Sanvito S, Levy O. The high-throughput highway to computational materials design. Nat Mater 2013;12:191.
[20] Galanakis I, Mavropoulos Ph, Dederichs PH. Electronic structure and SlaterPauling behaviour in half-metallic heusler alloys calculated from first principles. J Phys D: Appl Phys 2006;39:765.
[21] Wei X-P, Deng J-B, Mao G-Y, Chu S-B, Hu X-R. Half-metallic properties for the Ti_2YZ (Y = Fe,Co,Ni; Z = Al,Ga,in) heusler alloys: a first-principles study. Intermetallics 2012;29:86.
[22] van Leuken H, de Groot RA. Half-metallic antiferromagnets. Phys Rev Lett 1994;74:1171.
[23] Luo HZ, Zhang HW, Zhu ZY, Ma L, Xu SF, Wu GH, et al. Half-metallic properties for the Mn_2FeZ (Z = Al,Ga,Si,Ge,Sb) heusler alloys: a first-principles study. J Appl Phys 2008;103:083908.
[24] Hu X. HalfMetallic antiferromagnet as a prospective material for spintronics. Adv Mater 2011;24:294.
[25] Hussain MK. Investigations of the electronic and magnetic properties of newly (001) surface LiCrS and LiCrSe half-heusler compounds. Appl Phys A 2018;124:343.
[26] Wang X, Cheng Z, Liu G. Largest magnetic moments in the half-heusler alloys XCrZ (X = Li,K,Rb,Cs; Z = S,Se,Te): a first-principles study. Materials 2017;10:1078.
[27] Graf T, Felser Cl, Parkin SSP. Simple rules for the understanding of heusler compounds. Prog Solid State Chem 2011;39:1.
[28] Blaha, P.; Schwarz, K.; Madsen, G. K. H.; Kvasnicka, D.; Luitz, J.; Laskowski, R.; et al. WIEN2k, an augmented plane wave + local orbitals program for calculating crystal properties, karlheinz schwarz, techn. Universität Wien 2018, Austria, ISBN:3-9501031-1-2.
[29] Perdew JP, Burke K, Ernzerhof M. Generalized gradient approximation made simple. Phys Rev Lett 1996;77:3865.
[30] Tran F, Blaha P. Accurate band gaps of semiconductors and insulators with a semilocal exchange-correlation potential. Phys Rev Lett 2009;102:226401.
[31] Kresse G, Fürthmuller J. Efficient iterative schemes for ab initio total-energy calculations using a plane-wave basis set. Phys Rev B 1996;54:11169.
[32] Blöchl PE. Projector augmented-wave method. Phys Rev B 1994;50:17953.
[33] Alfè D. PHON: a program to calculate phonons using the small displacement method. Comput Phys Commun 2009;180:2622.
[34] Togo A, Tanaka I. First principles phonon calculations in materials science. Scripta Mater 2015;108:1.
[35] Singh A, Mohapatra S, Ziman T, Chatterji T. Spin waves in the FCC lattice antiferromagnet: competing interactions, frustration, and instabilities in the hubbard model. J Appl Phys 2017;121:073903.
[36] Escorihuela-Sayalero C, Diéguez O, Íñiguez J. Strain engineering magnetic frustration in perovskite oxide thin films. Phys Rev Lett 2012;109:247202.
[37] Cazorla C, Íñiguez J. Insights into the phase diagram of bismuth ferrite from quasiharmonic free-energy calculations. Phys Rev B 2013;88:214430.
[38] Cazorla C, Diéguez O, Íñiguez J. Multiple structural transitions driven by spin-phonon couplings in a perovskite oxide. Sci. Adv. 2017;3:e1700288.
[39] Cazorla C, Íñiguez J. Giant direct and inverse electrocaloric effects in multiferroic thin films. Phys Rev B 2018;98:174105.
[40] Webster PJ, Ziebeck KRA. In: Wijn HPJ, Landolt-Boörnstein, editors. Alloys and compounds of *d* -elements with main group elements. Part 2, vol. 19. Berlin: Pt. C Springer-Verlag; 1988. p. 75–184. New Series, Group III.
[41] Cazorla C, Boronat J. First-principles modeling of quantum nuclear effects and atomic interactions in solid ^{4}He at high pressure. Phys Rev B 2015;91:024103.
[42] Rost CM, Sachet E, Borman T, Moballegh A, Dickey EC, Hou D, et al. Entropy-stabilized oxides. Nat Commun 2015;6:8485.
[43] Benisek A, Dachs E. The vibrational and configurational entropy of disordering in Cu_3Au. J Alloy Comp 2015;632:585.
[44] Shenoy JN, Hart JN, Grau-Crespo R, Allan NL, Cazorla C. Mixing thermodynamics and photocatalytic properties of GaP-ZnS solid solutions. Adv. Theory Simul. 2019;2:1800146.
[45] van de Walle A, Ceder G. The effect of lattice vibrations on substitutional alloy thermodynamics. Rev Mod Phys 2002;74:11.
[46] Bhattacharya S, Madsen GKH. A novel P-type half-heusler from high-throughput transport and defect calculations. J Mater Chem C 2016;4:11261.
[47] Page A, Poudeu PFP, Uher C. A first-principles approach to half-heusler thermoelectrics: accelerated prediction and understanding of material properties. J. Materiomics 2016;2:104.
[48] Rogl G, et al. (V,Nb)-Doped half heusler alloys based on (Ti,Zr,Hf)NiSn with high ZT. Acta Mater 2017;131:336.

M. Atif Sattar is currently a Ph.D. student in the Islamia University of Bahawalpur, Pakistan. He was exchange student in the school of Material Science, UNSW, Sydney, Australia under IRSIPHEC, Pakistan for six months. His research focuses on the structural, electronic and magnetic properties of the half-metallic ferromagnets based on Heusler Alloys.

Dr. Cazorla was awarded his doctorate in Computational Physics by the Polytechnic University of Catalonia (Barcelona, Spain) in 2006. From 2006 to 2010, Dr. Cazorla worked as a postdoctoral researcher in the group of Prof. Michael Gillan and Prof. Dario Alfe at the University College London (London, United Kingdom). In 2010, Dr. Cazorla moved to the Institute of Materials Science of Barcelona (Barcelona, Spain) as a JAE-DOC Fellow. From 2015 to present, Dr. Cazorla is an ARC Future Fellow at the School of Materials Science and Engineering in UNSW Sydney. His primary research interest is the application and development of computational techniques to understand and predict new oxide-based and inorganic materials for nanoelectronics and energy conversion and storage applications.